Coherent Model for Cross-Polarization Coupling from a Single Point-Like Perturbation in Optical Fibers

Junhao Liu, Yongqing Yi, and Tianhua Xu, *Member, IEEE*

***Abstract*—The transfer matrix is proposed to describe the coherent cross-polarization coupling (CPC) induced by a single point-like perturbation (PLP) in optical fibers. This matrix remains independent of the fiber length, making it suitable for characterizing the PLP that have a zero-dimensional impact on fiber length. Consequently, the fiber can be fully characterized by a matrix combining the transfer matrix of CPC and the Jones matrix of the fiber birefringence. The polarization performance of fibers exhibiting both CPC and birefringence is analyzed using the developed combined model.**

***Index Terms*—Birefringence, Cross-polarization coupling, Jones matrix, Optical fibers, Polarization cross talk, Polarization extinction ratio, Transfer matrix.**

I. Introduction

CROSS-POLARIZATION COUPLING (CPC) is a factor limiting the performance of single-mode fibers (SMFs) [1], [2], especially the interferometric sensor employing them such as fiber-optic gyroscopes (FOGs) [3]-[5]. It is from the mode coupling between the two orthogonal polarizations of the fundamental mode, i.e., the eigen polarization modes [6] or the principal states of polarization [7]. It causes the polarization mode dispersion [8], polarization fluctuation [9], and polarization noise [10] in fiber telecommunication and sensing applications. The very weak CPC in SMFs is induced by the fluctuations in the effective refractive index of the fiber, which is from the tiny imperfection in the manufacturing process [11]. However, it is quite sensitive to various environmental perturbations such as thermal, magnetic, and stress fields, which degrade the CPC in SMFs [12] - [14]. To prevent the CPC aggravation from those external perturbations, a special SMF, polarization-maintaining fibers (PMFs) was developed for interferometric fiber applications [15]. The input polarization of PMFs is usually one of the two orthogonal eigen or principal states of polarization, which is linearly polarized along one of the two principal axes of fiber birefringence [16]. It could be hold unchanged during the propagation along the PMF, since its intrinsic linear birefringence is high and could resistance the CPC degradation from external perturbations [11], [13] - [17]. This polarization maintaining ability makes the PMF suitable to interferometric fiber sensors such as FOGs [18]. Then the CPC represents the quality of a PMF [15], i.e., its immunity against environments, and hence the corresponding system performance employing them [19]. Unfortunately, it was found recently that the birefringence intrinsic to the PMF itself can be another error source for high performance FOGs [20], [21].

The CPC in fibers is described by two similar parameters, polarization cross talk (PCT) [22] and polarization extinction ratio (PER) [23]. Both parameters are from the ratio of optical powers in the two output polarizations under the condition that only one of them was inputted. For the weak CPC case of interest, most power remains in the input polarization, major polarization, and few are coupled by the CPC into the orthogonal, minor polarization. Early works established a random coupling model for the CPC in fibers to mathematically calculate the PER or PCT. The model assumed that there are many point-like perturbations (PLPs) distributed along the fiber length. It explained the PER of the fiber as the statistic result of CPC from all these PLPs. However, the PER or PCT of the CPC from a single PLP and its physical mechanism, which should be the base of the model, were not reported yet. Meanwhile, there are two assumptions in the early CPC model, and both make the model not accurate enough. The first is based on the idea that only one polarization (the major polarization) is excited at the input, and the power in the other polarization (the minor polarization) is zero. It is obviously impossible to achieve this ideal inputting condition of linear polarization in practice. The second is that the CPC is unidirectional, i.e., there is only the CPC from the major to the minor polarizations in the fiber. The opposite CPC, i.e., the CPC from the minor to the major polarizations, was typically not considered. This assumption holds true only in the situation of the weak CPC. In reality, the weak CPC intrinsic to the fiber can become significant under some external environment such as temperature variations, especially for the coiled fiber in fiber sensors. As a result, the PER or PCT of a real fiber never be theoretically calculated, only can be measured [24], [25].

This work was supported by EU Horizon 2020 MSCA Grant 101008280 (DIOR) and UK Royal Society Grant (IES\R3\223068). (Corresponding authors: Junhao Liu and Tianhua Xu)

J. Liu is with Tianjin Institute of Electronic Materials, Tianjin 300220, China (e-mail: uceexux@ucl.ac.uk).

Y. Yi is with Tianjin Key Laboratory of Special Materials for Optical Fibers, Tianjin 300220, China (e-mail: plan@emri46.com.cn).

T. Xu is with School of Engineering, University of Warwick, United Kingdom, is also with University College London, United Kingdom, and is also with Tianjin University, Tianjin 300072, China (e-mail: tianhua.xu@ieee.org).

On the other hand, there has not been a unified description for both birefringence and CPC simultaneously existed in the fiber. It is due to the lack of mathematical relation between them, since that models for them are independently established and separately used in early works. The model for birefringence was represented in terms of two amplitudes of the orthogonal polarizations, treating the fiber as a sequence of two lumped optical elements [26]. In contrast, the CPC model was described in terms of powers of the orthogonal polarizations [11]. The early CPC model depended on fiber length, which typically included multiple PLPs, and the CPC induced by a single PLP has not been analytically calculated or predicted. At the same time, the independence of the two models have been responsible for the fact that birefringence and CPC of a fiber have never been considered simultaneously, but individually and separately, such as their effect on FOGs [4], [5], [20], [21], [27].

In this paper, we have developed a comprehensive model for calculating the CPC from a single PLP for improving the accuracy of FOGs. This model characterizes both the amplitude and phase of the CPC using a transfer matrix, and can be seamlessly integrated with the existing fiber birefringence model. The combined model provides a complete description of a fiber exhibiting both birefringence and CPC. Numerical results, based on this proposed model, demonstrated that the position and the strength of the CPC, the linear and circular birefringence of the fiber, as well as the initial phase and the PER of the input light, are crucial to the measured CPC of the fiber.

II. THEORY

The matrix representation of a fiber in this section has been extended to encompass both the CPC originating from a PLP and the distributed birefringence along the fiber, utilizing the principles of Jones calculus.

A. Jones calculus for a fiber with birefringence

According to Jones [28], the propagation of field in an optical system such as a fiber could be described by

$$\mathbf{E}' = \mathbf{M}\mathbf{E}, \tag{1}$$

where

$$\mathbf{E}' = \begin{pmatrix} E_x' \\ E_y' \end{pmatrix} \quad \text{and} \quad \mathbf{E} = \begin{pmatrix} E_x \\ E_y \end{pmatrix} \tag{2}$$

are Jones vectors of the output and input fields, respectively, which are expressed by complex amplitudes of the two basis orthogonal polarizations, i.e., denoted by x - and y - polarizations here, respectively. Jones matrix of the system is

$$\mathbf{M} = \begin{pmatrix} m_{11} & m_{12} \\ m_{21} & m_{22} \end{pmatrix}. \tag{3}$$

There are relationships of $m_{12} = m_{21}$ and $m_{22} = m_{11}^*$ for the Jones matrix established in the fixed laboratory coordinate system.

According to Kapron [26], for the optical propagation in a fiber with a given length L, the fiber can be represented as an equivalent cascade of two lumped elements. One is a retarder with linear retardation $\Delta\beta L$, where

$$\Delta\beta = \beta_x - \beta_y = \frac{2\pi}{\Lambda}, \tag{4}$$

is the difference in propagation constants of the slow and the fast axes for the linear birefringence of the fiber, i.e., β_x and β_y here, respectively, and Λ is beat length. Then Jones matrix of the linear birefringence in the fiber can be written as [20]

$$\boldsymbol{\beta}_L = e^{i\bar{\beta}L} \begin{pmatrix} e^{i\Delta\beta L/2} & 0 \\ 0 & e^{-i\Delta\beta L/2} \end{pmatrix}, \tag{5}$$

where

$$\bar{\beta} = \left(\beta_x + \beta_y\right)/2, \tag{6}$$

is the mean propagation constant of the fiber. The other is a rotator with a polarization rotation αL, where [20]

$$\alpha = g\xi \tag{7}$$

is the circular birefringence through photo-elastic effect induced by the fiber twisting at rate ξ, here $g = -0.17$ is the material constant of the fiber core.

Then Jones matrix of the circular birefringence for the fiber can be written as

$$\boldsymbol{\alpha}_L = \begin{bmatrix} \cos(\alpha L) & \sin(\alpha L) \\ -\sin(\alpha L) & \cos(\alpha L) \end{bmatrix}. \tag{8}$$

Here, it is assumed that the positive polarization rotation follows a counterclockwise direction. There is no circular birefringence resulting from the internal rotation of birefringence axes in PMFs in (8), which differs from our previous work [20]. Since the internal rotation occurs at the melt temperature during the fiber drawing, and there is no stress to support photo-elastic effect.

The birefringence matrix of the fiber be written as a rotator followed by a retarder [26]

$$\mathbf{B}_L = \boldsymbol{\beta}_L \boldsymbol{\alpha}_L = e^{i\bar{\beta}L} \begin{pmatrix} A & B \\ -B^* & A^* \end{pmatrix}, \tag{9}$$

or the matrix from the reversed order as pointed out in [20],

$$\mathbf{B}_L' = \boldsymbol{\alpha}_L \boldsymbol{\beta}_L = e^{i\bar{\beta}L} \begin{pmatrix} A & B^* \\ -B & A^* \end{pmatrix}, \tag{10}$$

where the elements are

$$\begin{aligned} A &= e^{i\Delta\beta/L}\cos(\alpha L) \\ B &= e^{i\Delta\beta/L}\sin(\alpha L) \end{aligned} \tag{11}$$

for the fiber with linear birefringence (4) and circular birefringence (7) uniformly distributed on its length L.

Three notes should be addressed here.

Firstly, the relationships between the elements of birefringence matrices (9) and (10) for a fiber are different from the original Jones matrix (3) of a bulk optics. This difference arises because that the original Jones matrix was established in the fixed laboratory coordinate system, which necessitates the use of a second rotation matrix with an opposite sense for detecting the output light. Conversely, the birefringence matrix of a fiber is defined within the principal axes coordinate system of its linear birefringence, where the second rotation matrix is

not necessary since the system is already rotated by the circular birefringence inherent to the fiber itself at the output end.

Secondly, the relationship between matrices (9) and (10) involves a mutual transposition with a negative sign for off-diagonal elements, as opposed to a pure transpose, as we previously demonstrated in [20]. This difference arises from the invariance introduced by a helix due to the circular birefringence distributed along the fiber length. The concept of a pure transpose is derived from the original Jones matrix, where off-diagonal elements remain unchanged. This distinction is particularly important in systems involving counter-propagations, such as FOGs, where most early studies utilized the pure transpose approach.

Thirdly, in practical measurements of PCT or PER for a fiber, a manually rotatable analyzer in optical path or an automatically one is integrated in the setups. Such an analyzer ensures that all measurements are consistently performed within the principal axes coordinate system of the fiber linear birefringence. Consequently, matrix (9) or (10) should be employed consistently in these measurements. We have used the form presented in (9) for the sake of clarity.

B. *Transfer matrix of the CPC from a single PLP*

Here, we propose the transfer matrix to describe the CPC induced by a single PLP (zero dimension in fiber length) as shown in Fig. 1 by analogy. Assuming that the CPC is symmetric and lossless, there is a transfer matrix for the CPC with a real number for the CPC ratio χ in $0 \le \chi \le 1$:

$$\boldsymbol{\chi} = \begin{bmatrix} \sqrt{1-\chi} & -e^{i\phi}\sqrt{\chi} \\ -e^{i(\pi-\phi)}\sqrt{\chi} & \sqrt{1-\chi} \end{bmatrix}, \tag{12}$$

where ϕ is the phase shift of CPC with $0 \le \phi \le \pi$. The sum of the two phase shifts for CPC, one from the major to the minor polarization and the other for opposite CPC from the minor to the major polarization, π, is determined from the relationship between phase shifts associated with the refraction and the transmission of a beam splitter [29]. It could be confirmed that the law of energy conservation is satisfied for $\boldsymbol{\chi}$ given in (12) by simply calculating the optical powers before and after the CPC. This shows the theoretical validity of the matrix (12) for the CPC from a single PLP.

It is noted that the CPC transfer matrix (12) also can be written as

$$\boldsymbol{\chi} = \begin{pmatrix} \sqrt{1-\chi} & -e^{i\phi}\sqrt{\chi} \\ e^{-i\phi}\sqrt{\chi} & \sqrt{1-\chi} \end{pmatrix} \tag{13}$$

by trigonometric equalities. It shows clearer relationships between its elements. Specifically, two important relationships emerge: (i) conjugate between diagonal elements and (ii) negative conjugate between off-diagonal elements. These relationships in the CPC transfer matrices (12) and (13) align perfectly with those in the birefringence matrices (9) and (10). The alignment shows the non-reciprocity of the CPC from the same PLP within a fiber for both forward and backward propagations such as in FOGs. It is from the presence of identical relationships in the CPC matrices as observed in the birefringence matrices between the forward and backward propagations.

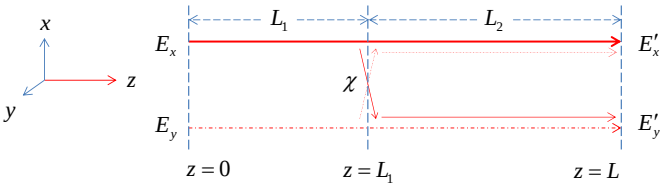

Fig. 1. Schematic diagram of the CPC from a single PLP in optical fibers. The PLP located at $z = L_1$ from the input end $z = 0$. It divides the original fiber length L into two sections of length L_1 and L_2 with the same linear birefringence $\Delta\beta = 2\pi/\Lambda$ and circular birefringence α. At the output end $z = L$, field in each polarization is the linear superposition of two parts: the remained original and the coupled orthogonal polarizations.

C. *Transfer matrix of a fiber with birefringence and a CPC*

Using the Jones matrix for the fiber birefringence and the transfer matrix for the CPC, the transfer matrix of a fiber with birefringence and CPC can be written as

$$\mathbf{M} = \mathbf{B}_2' \boldsymbol{\chi} \mathbf{B}_1, \tag{14}$$

with

$$\begin{aligned} m_{11} &= \sqrt{1-\chi}\left(A_2A_1 - B_2^*B_1^*\right) - \sqrt{\chi}\left[e^{i(\pi-\phi)}B_2^*A_1 + e^{i\phi}A_2B_1^*\right] \\ m_{12} &= \sqrt{1-\chi}\left(A_2B_1 + B_2^*A_1^*\right) - \sqrt{\chi}\left[e^{i(\pi-\phi)}B_2^*B_1 - e^{i\phi}A_2A_1^*\right] \\ m_{21} &= -\sqrt{1-\chi}\left(B_2A_1 + A_2^*B_1^*\right) - \sqrt{\chi}\left[e^{i(\pi-\phi)}A_2^*A_1 - e^{i\phi}B_2B_1^*\right] \\ m_{22} &= -\sqrt{1-\chi}\left(B_2B_1 - A_2^*A_1^*\right) - \sqrt{\chi}\left[e^{i(\pi-\phi)}A_2^*B_1 - e^{i\phi}B_2A_1^*\right] \end{aligned}, \tag{15}$$

where A_1, B_1, and A_2, B_2 are from (11) with corresponding fiber length shown in Fig. 1. It can be shown that there still exist $m_{21} = -m_{12}^*$ and $m_{22} = m_{11}^*$ as in (9) or (10), and (12) or (13), indicating the non-reciprocity of the fiber with both birefringence and CPC for opposite propagations. This mirrors what is observed in cases of pure birefringence (without CPC), as discussed in reference [20].

D. *Measured PCT and PER of the output light*

In practical measurements, the PER η is usually defined by the maximum power $P_{\max}$ and the minimum power $P_{\min}$ as

$$\eta = -10\log\frac{P_{\min}}{P_{\max}} = 10\log\frac{P_{\max}}{P_{\min}} > 0, \tag{16}$$

and the extreme powers are polarized in orthogonal directions. On the other hand, the PCT γ is also defined by the same extreme powers as

$$\gamma = 10\log\frac{P_{\min}}{P_{\max} + P_{\min}} < 0. \tag{17}$$

Obviously, there is $\eta + \gamma \approx 0$ when $\eta = -\gamma \ge 10$ dB, which is of significant interest in practice. In following we take PER for simplicity.

By assuming the initial phase difference δ between the input orthogonal polarizations, the minor polarization E_y with the minimum power $P_{\min}$ could be expressed in the major

polarization E_x with the maximum power $P_{\max}$ through input PER η as

$$E_y = 10^{-\eta/20} E_x e^{i\delta}. \quad (18)$$

Substituting (18) into (1) and employing (14)-(16) we finally get the output PER η' of a fiber with a single CPC under the input PER η is

$$\eta' = -10\times \log \frac{m_{21}m_{21}^* + 10^{-\eta/10} m_{22}m_{22}^* + 10^{-\eta/20}\left(m_{21}^* m_{22} e^{i\delta} + m_{21} m_{22}^* e^{-i\delta}\right)}{m_{11}m_{11}^* + 10^{-\eta/10} m_{12}m_{12}^* + 10^{-\eta/20}\left(m_{11}^* m_{12} e^{i\delta} + m_{11} m_{12}^* e^{-i\delta}\right)}. \quad (19)$$

Equation (19) analytically links the output PER to the properties and the input light of the fiber. It contains all factors influencing the measurement of CPC in fibers.

III. Results

Using the developed analytical model of the CPC in optical fibers, the output PER could be numerically calculated using MATLAB to show the effects of various factors on the output PER.

A. *Strength of the CPC*

Figure 2 illustrates the impact of CPC strength across its entire range under various input PER. As expected, the output PER consistently decreases as the coupling strength increases. The symmetry observed in the output PER values with respect to zero dB output PER ($\eta' = 0$ dB) confirms the presence of opposite coupling from the minor to the major polarizations. It occurs at CPC ratio $\chi = 0.5$ for any input PER. Furthermore, apart from this special ratio, higher input PER values lead to higher output PER values at any fixed CPC ratio. This highlights the first requirement for accurate CPC measurement, emphasizing the need for a high input PER, as originally assumed an ideal input (single polarization).

The negative values of output PER observed when $\chi > 0.5$ occur due to the power exchange between the major and the minor polarizations resulting from the strong coupling at this region. It also gives out the second requirement for the precise CPC measurement. There should be $\chi \le 0.5$ to ensure a correct measurement since the instrument cannot distinguish between powers in slow polarization (P_x) and in fast polarization (P_y), can only distinguish between $P_{\max}$ and $P_{\min}$ i.e., the maximum and the minimum of optical power, respectively. When there exists $\chi > 0.5$ (the output PER $\eta' < 3$ dB) for strong coupling, we will not be able to tell whether the CPC ratio is χ or $1-\chi$.

Figure 3 depicts a scenario of particular interest with weak CPC, which is prevalent in most situations. For the sake of convenient comparison, the CPC ratio here is presented in logarithm form (dB), which corresponds to the PCT. In this figure, there are two approximated linear parts (ALPs)

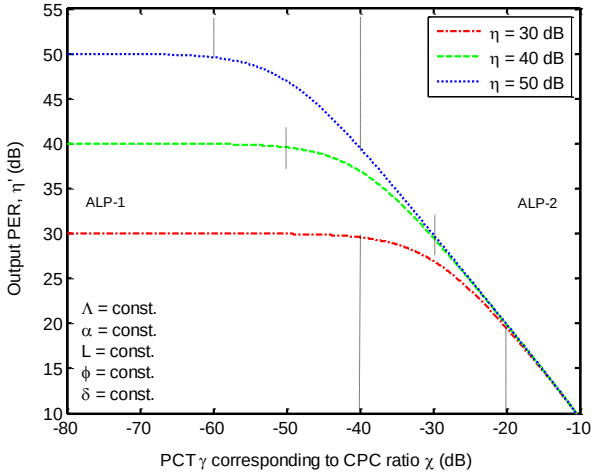

Fig. 3. Dependency of output PER on PCT corresponding to CPC ratio. There are three parts in all curves: a nonlinear part at the middle region where input PER is comparable to CPC, two ALPs at the opposite end where input PER far away from CPC. The output PER is close to the lower one in the two ALPs. A proper range for the nonlinear part is $\gamma \pm 10$ dB.

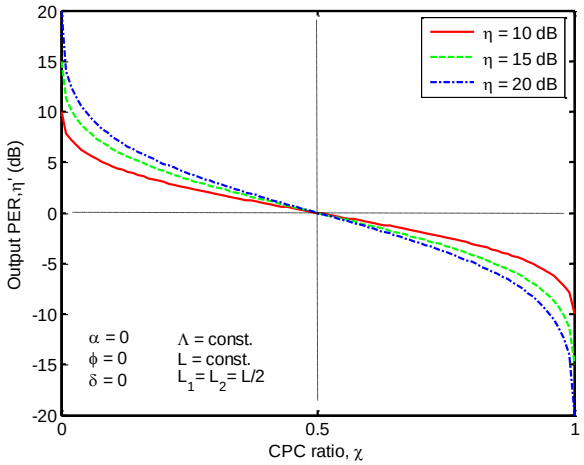

Fig. 2. Dependency of output PER on CPC ratio. The output PER becomes lower when CPC ratio is higher. High input PER gives high output PER for any fixed CPC ratio. The output PER is 0-dB at CPC ratio $\chi = 0.5$ for any input PER.

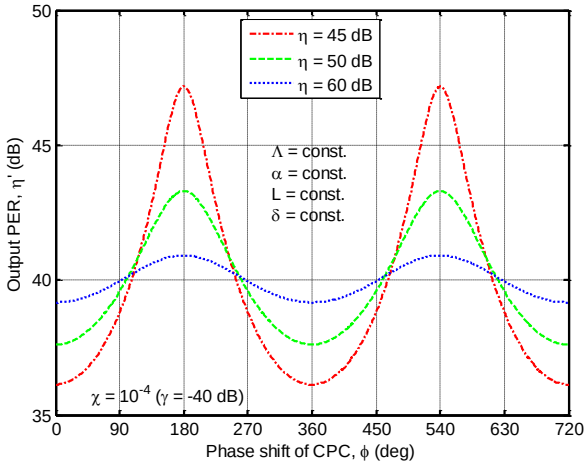

Fig. 4. Dependency of output PER on the phase shift of CPC when input PER is higher than CPC itself. The input PER is lower (closer to CPC), the resonance of output PER is larger. Maxima of output PER are higher than the CPC itself, which shows the interference of the coherent model.

noticeable. The first one (ALP-1) pertains to cases where the input is exceedingly low on the left side, resulting in the output being equal to the input PER due to relatively weak coupling. Conversely, the second (ALP-2) is associated with situations where the coupling is much stronger compared to the input, as observed in the rightmost portion of Fig. 3. The third portion, situated between the two ALPs, exhibits a significant non-linear decline. The non-linear segment typically occurs at approximately ± 10 dB outside of the CPC region. The interference phenomena occur in this non-linear portion, as will be discussed in the subsequent section to consider the phase shift of the CPC.

The linear birefringence denoted by beat length Λ, circular birefringence α, and length L of the fiber, as well as phase shift ϕ of the CPC, and initial phase difference δ of the input polarizations, are all considered as constants, i.e., could be predefined with arbitrary values.

B. Phase shift of the CPC

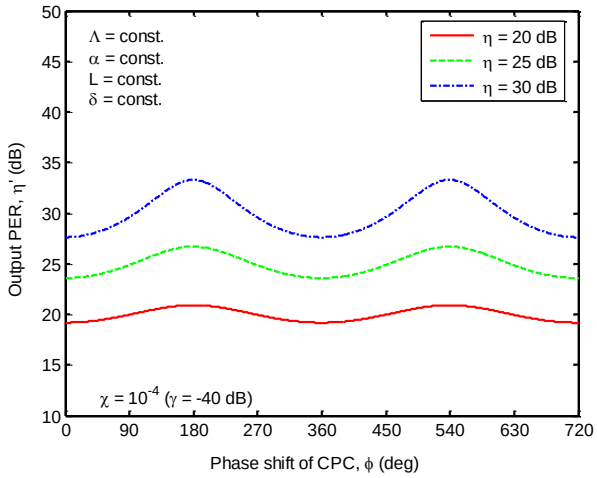

Fig. 5. Dependency of output PER on the phase shift of CPC when input PER is lower than CPC itself. The input PER is higher (closer to CPC), the oscillation of output PER is larger. Maximums of output PER are lower than the CPC itself, which means the output reflects the input, instead of the CPC.

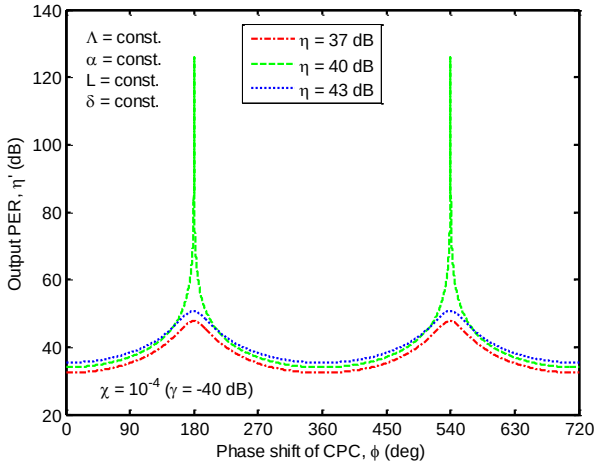

Fig. 6. Dependency of output PER on position of on the phase shift of CPC when input PER is comparable to CPC itself. The resonance occurs when input PER (40-dB) is equal to CPC itself ($\chi = 10^{-4}$ or $\gamma = -40$ dB).

Figures 4, 5, and 6 show the influence of the phase shift ϕ of CPC with a constant weak coupling ($\chi = 0.0001$ or $\gamma = -40$ dB) for three high (45, 50, and 60-dB), low (20, 25, and 30-dB), and comparable (37, 40, and 43-dB) input PERs, respectively. They are under constant birefringence and fiber length with arbitrary values. They represent the initial phase difference $\delta = 0$ between orthogonal polarizations of the input light, given their sensitivity to this parameter. The range of phase shift ϕ of the CPC is extended for the sake of clarity and improved observation.

There are obvious but special periods: they are not symmetric between maxima at $(2n-1)\pi$ (here $n = 1, 2, 3, \ldots$) and minima at $2n\pi$. Firstly, the distances of these points to the real CPC (40-dB here) are different. For the distances to the CPC, the maxima' are farther than the minima'. Secondly, the peaks above the CPC are narrower compared to the troughs below it. The unique pattern suggests a larger probability for the minima in practical measurements, which shows a lower output PER than the CPC. The periodic behavior comes from

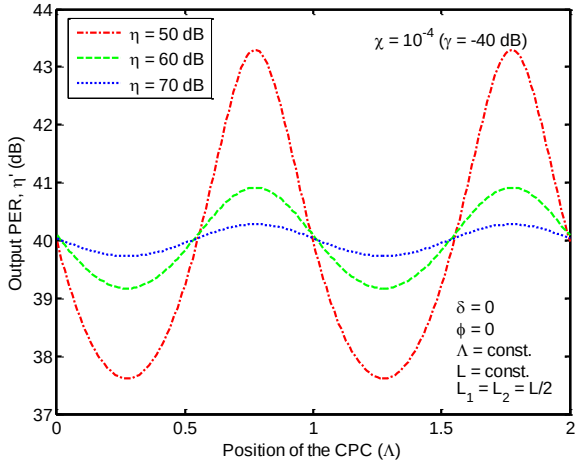

Fig. 7. Dependency of output PER on position of the PLP for high input PER. The positions are given by the beat length of linear birefringence for a clear demonstration.

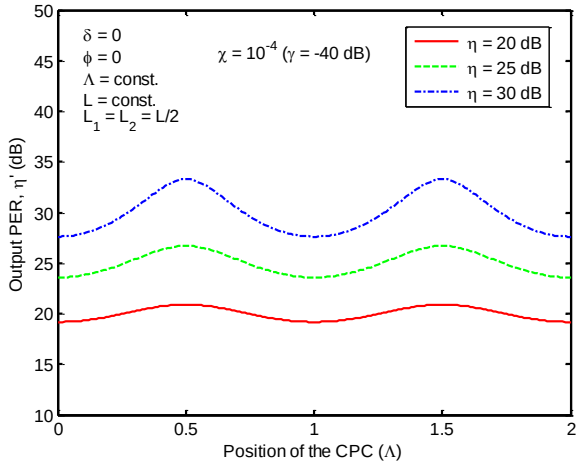

Fig. 8. Dependency of output PER on position of the PLP for low input PER. The positions are given by the beat length of linear birefringence for a clear demonstration.

the interference in superposition of the remained original signals with the coupled orthogonal polarization. Another piece of evidence supporting the interference is that the maximum output PER for the lower input PER is higher than that for higher input PER. It exceeds the input PER itself for the 45-dB input, since it is closer to the real CPC (40-dB).

There are indeed probabilities of observing the real CPC for all higher input PERs, as evidenced by the fact that all curves intersect at 40-dB, as illustrated in Fig. 4. Conversely, for lower input PER values, as illustrated in Fig. 5, there are no probabilities of encountering the real CPC. Resonance phenomena occur precisely when the input equals to the CPC itself, resulting in the spikes observed in Fig. 6, which are from the interference in this coherent model for CPC. These spikes are a consequence of the interference effects presented in this coherent model for CPC. It could be predicted that the resonance will occur again due to the birefringence of the fiber. In the subsequent analysis, we will focus on cases involving higher and lower inputs to avoid resonances near the point of equality. These higher and lower input cases correspond to the CPC originating from a single PLP and a whole fiber with multiple PLPs, respectively.

C. *Position of the CPC*

Figures 7 and 8 show the effects of the PLP position where the CPC occurs for high and low input PERs, respectively. The position is expressed via the beat length of linear birefringence for a clear demonstration. There are more clear interferences for lower and higher input PER in Figs. 7 and 8, respectively, i.e., closer to CPC itself, as expected from the coherent model. The interference period precisely corresponds to the beat length of the linear birefringence in fibers.

The similarity between Figures 7 and 4, as well as 8 and 5 indicated the influence of phase on the output PER in the coherent scenario. There are also resonances similar to Fig. 6 for the effect of CPC position on the output PER when input PER is comparable to the CPC itself. The rare resonance phenomenon occurring in the special case when input PER is

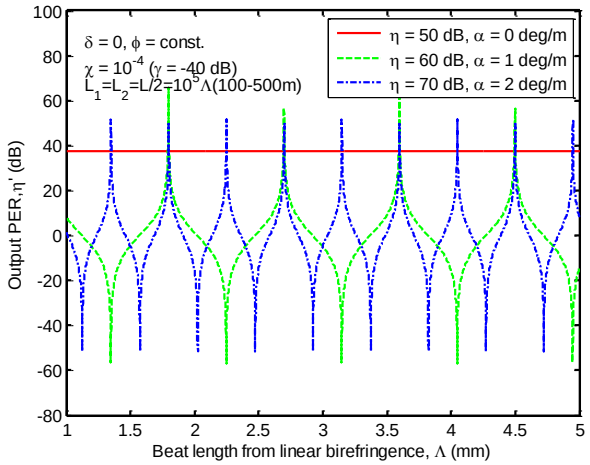

Fig. 9. Dependency of output PER on beat length from linear birefringence under different circular birefringence and high input PER. The periodical variations are from nonzero circular birefringence, and more periods are from higher circular birefringence for constant fiber length.

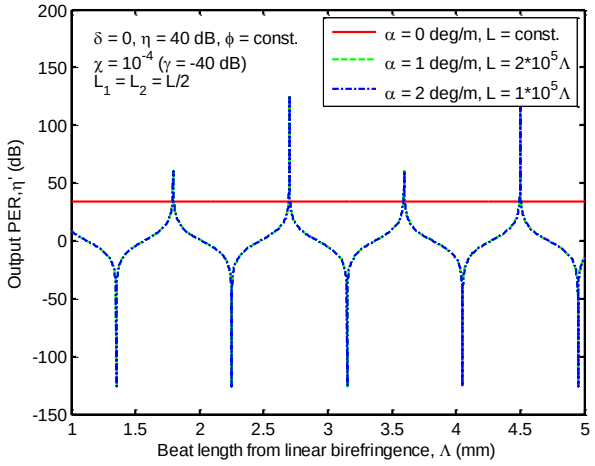

Fig. 10. Dependency of output PER on beat length from linear birefringence under different circular birefringence and same input PER. The periodical variations come from nonzero polarization rotation (product of circular birefringence and fiber length).

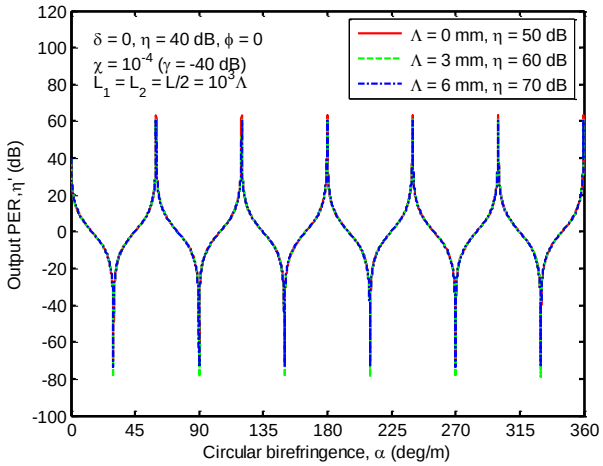

Fig. 11. Dependency of output PER on circular birefringence of the fiber under difference beat length (linear birefringence). The perturbation point is located at the middle point of the fiber length. There are same periods and extreme values for different linear birefringence and input PER. The same periods are from the same fiber length, on which the polarization rotation from the circular birefringence (fiber twist) is accumulated.

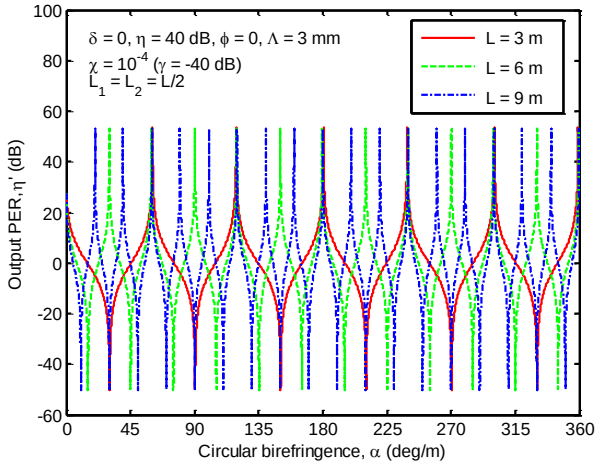

Fig. 12. Dependency of output PER on circular birefringence of the fiber under same beat length (linear birefringence) for different fiber length. The numbers of periods are proportional to the fiber length.

close to CPC ratio is not show here again and hereafter.

D. *Linear birefringence of the fiber*

Figures 9 and 10 illustrate the influence of the linear birefringence on output PER for both higher and lower input PER values, respectively. In both cases, there is periodic dependency introduced by the presence of nonzero circular birefringence. When the fiber is untwisted, meaning that circular birefringence is zero, the output PER remains constant, as shown by $\alpha = 0$ in both figures. This observation suggests that the periodic dependency of output PER indeed arises from the nonzero circular birefringence inherent to the fiber. Conversely, the magnitude of the constant output PER is affected by the linear birefringence and the CPC characteristics of the fiber under the same fiber length. Curves for $\alpha = 1$ deg/m and $\alpha = 2$ deg/m for same length in Fig. 10 and different length in Fig. 9 indicate that this periodicity comes from the polarization rotation, i.e., the accumulation of circular birefringence over the fiber length.

E. *Circular birefringence of the fiber*

Figures 11 and 12 show the effects of circular birefringence of the fiber for different linear birefringence and fiber lengths, respectively. The PLP is located at the middle of the fiber length, and the CPC ratio is constant at $\chi = 10^{-4}$ (corresponding to a PCT of $\gamma = -40$ dB). The input PER for both figures is set at $\eta = 40$ dB, which equals the CPC itself. Resonances at peaks in these figures are obvious. For a constant fiber length, the linear birefringence of the fiber does not influence the output, as shown in Fig. 11. For a constant linear birefringence, the longer fiber length results in more periods of output oscillation, as shown in Fig. 12, which arise from the accumulations of the retardation and rotation induced by the linear and the circular birefringence of the fiber.

F. *Initial phase of the input light*

Figures 13 and 14 show the effects of the initial phase difference between the orthogonal polarizations of the input

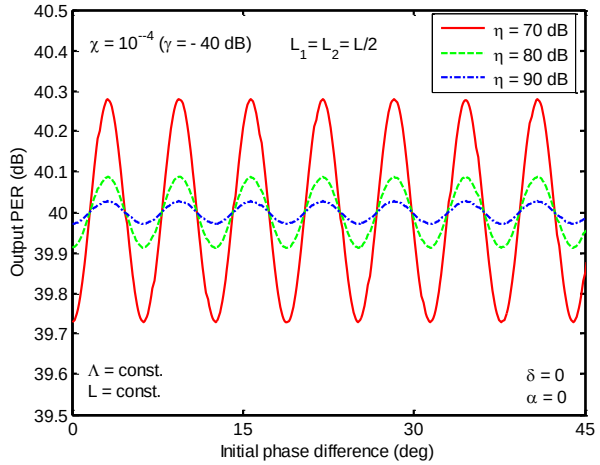

Fig. 13. Dependency of output PER on initial phase difference between orthogonal polarizations of input light for input PER higher than CPC ratio. Peaks are clearer for lower input PERs, i.e., closer to CPC ratio itself, in which resonances are easier to occur.

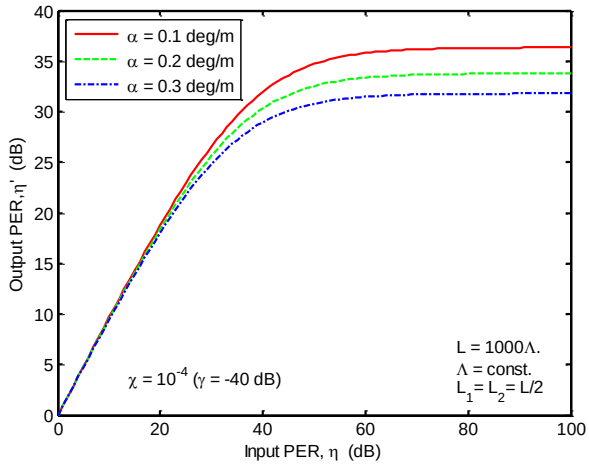

Fig. 15. Dependency of output PER on input PER for a fixed CPC ratio. The same tendency of them under small circular birefringence is similar to dependency on CPC ratio shown in Fig. 3. CPC measurements need an input PER higher than CPC ratio.

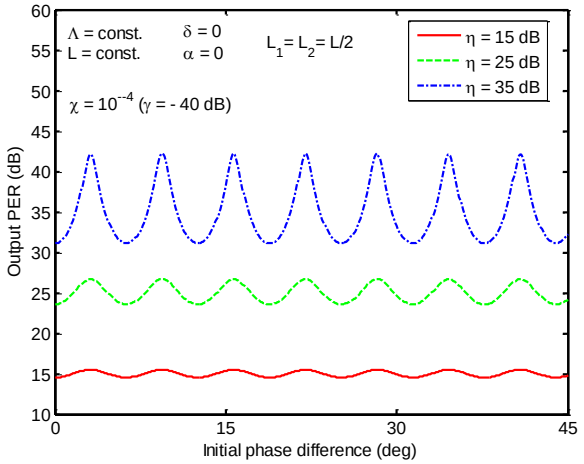

Fig. 14. Dependency of output PER on initial phase difference between orthogonal polarizations of input light for input PER lower than CPC ratio. Peaks are clearer for higher input PERs, i.e., closer to CPC ratio itself, in which resonances are easier to occur.

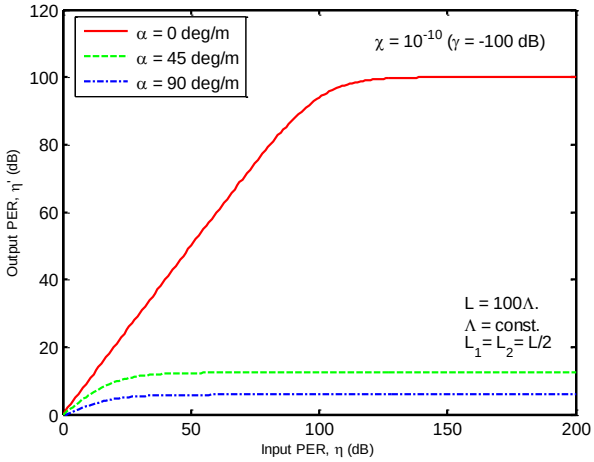

Fig. 16. Dependency of output PER on input PER for a fixed CPC ratio. Circular birefringence from fiber twist dominates the output PER when input PER is higher than CPC ratio.

light for high and low input PERs, respectively. A single PLP with CPC ratio $\chi = 10^{-4}$ ($\gamma = -40$ dB) is located at the middle of the fiber length again. There are seven periods for the initial phase differences in the ranges of from 0° to 45°. It does not depend on the length and the linear birefringence of the fiber. Lower input PERs in Fig. 13 and higher input PERs in Fig. 14 (closer to CPC ratio) result larger amplitudes of interference again. Phase shift on CPC and circular birefringence will translate the curves parallel to abscissa and ordinate axes, respectively, while maintaining the period invariant. However, the circular birefringence also influences the amplitude of the oscillation in all curves.

G. PER of the input light

Figures 15 and 16 show the effects of input PER on the output PER for different linear and circular birefringence when the PLP with a CPC ratio $\chi = 10^{-4}$ ($\gamma = -40$ dB) and $\chi = 10^{-10}$ ($\gamma = -100$ dB) is located at the middle of the fiber length, respectively. It can be seen that the circular birefringence from the fiber twist contributes the significant drop of the output PER, in addition to the impact of the CPC itself shown in Fig. 2 and, notably Fig. 3. It also reaffirms the importance of the input PER in practical measurements.

IV. Discussion

The advantage of the coherent model for the CPC in optical fibers is that it could be combined with birefringence model to completely describe the fiber, which is promising for fiber-optic interferometers such as FOGs. The limitation of the model is that it is too complicated to calculate the CPC from a real fiber with multiple PLPs instead of a single one.

There are a few methods to verify the coherent model proposed here for the CPC in optical fibers.

The basic method is using fiber-optic interferometers such as FOGs. A single PLP should be intentionally introduced in the arm of the balanced interferometer in this method. The phase shift and coupling ratio of the CPC induced by the PLP could be detected by the optical interference. Actually the performance of a FOG is influenced by the synthetic of both birefringence and CPC of the coiled fiber, in which specific crossovers are introduced by fiber coiling. The crossover in coiled sensing fibers is a typical PLP inducing CPC, which should be described by the present model. Multiple crossovers are inevitable for the coiled fiber in FOGs, and their description will be addressed by simplified the coherent model into an inherent one to calculate multiple PLPs in a further work.

An alter method is the PER measurement of a fiber also under an intentional PLP. In this method only the CPC ratio of the PLP could be investigated, since phase information is not included in the routine PER measurements.

There still are two works to be done for the conduction of methods mentioned above. One is the intentional and controllable PLP to be introduced on the fiber. A feasible PLP is the lateral pressure on a sufficiently small section of the fiber. It could be introduced by tailored clamps with quantifiable surface and pressure. The other is the physical mechanism of the CPC induced by the PLP, which is still not found now. Both will be addressed in our further works.

V. Conclusion

By proposing a transfer matrix for the cross-polarization coupling from a single point-like perturbation in optical fibers, shown that the output polarization of the fiber strongly depends on the strength and the phase shift of the CPC, the position along the fiber length of the perturbation point, the linear and the circular birefringence of the fiber, as well as the input polarization and the initial phase difference between the two orthogonal polarizations of the input light. The analytical model combined the cross-polarization coupling and birefringence of the fiber. It provides a complete description for the polarization property of optical fibers. It also highlights the need for thoroughly considering these factors in design and analysis of optical fiber systems and its measurements.

References

[1] Z. Yu, J. Yang, C. Lin. X. Zhang, F. Dang, Y. Yuan, L. Yuan, Y. Wang, and Y. Qin, "Distributed polarization measurement for fiber sensing coils: a review," *J. Lightw.Technol.*, vol. 39, no.12, pp. 3699-3710, Jun. 2021.

[2] X. Wang, C. Zhao, H. Wu, R. Liao, W. Chen, and M. Tang, "Fading-free polarization-sensitive optical fiber sensing," *Opt. Express*, vol. 28, no. 25, pp. 37334-37346, Dec. 2020.

[3] H. Zhang, Y. Yuan, Y. Zhu, F. Dang, Z. Yu, J. Yang, Y. Wang, and Y. Qin, "Distributed Polarization characteristic testing for optical closed loop of Sagnac interferometer," *J. Lightw. Technol.* vol. 40, no. 8, pp. 2548-2555, Apr. 2022.

[4] Y. Yang, H. Yan, S. Li, F. Yang, and W. Jin, "Estimation of gyro bias drift due to distributed polarization cross coupling in the fiber coil," *Opt. Express*, vol. 27, no.7, pp. 10247-10257, Apr. 2019.

[5] J. N. Chamoun and M. J. F. Digonnet, "Noise and bias error due to polarization coupling in a fiber optic gyroscope," *J. Lightw. Technol.*, vol. 33, no. 13, pp. 2839–2847, Jul. 2015.

[6] J. Sakai, S. Machida, and T. Kimura, "Existence of eigen polarization modes in anisotropic single-mode optical fibers," *Opt. Lett.*, vol. 6, no. 10, pp. 496-498, Oct. 1981.

[7] F. Curti, B. Daino, G. Marchis, and F. Matera, "'Statistical treatment of the principal states of polarization in single-mode fibers," *J. Lightw. Technol.*, vol. 8, no. 8, pp. 1162-1166, Aug. 1990.

[8] Y. Suetsugu, T. Kato, and M. Nishimura, "Full characterization of polarization mode dispersion with random mode coupling in single-mode optical fibers," *IEEE. Phot. Technol. Lett.*, vol. 7, no. 8, pp. 887-889, Aug. 1995.

[9] F. Tian, Y. Wu, P. Ye, "Analysis of polarization fluctuation in single-mode optical fibers with continuous random coupling," *J. Lightw. Technol.*, vol. 5, no. 9, pp. 1165-1168, Jan. 1987.

[10] N. C. Pistonl and M. Martinelli, "Polarization noise suppression in retracing optical fiber circuits," *Opt. Lett.*, vol. 16, no. 10, pp. 711-713, May 1991.

[11] I. P. Kaminow, "Polarization in optical fibers," *IEEE J. Quantum Electron.*, vol. 17, no.1, pp. 15-22, Jan. 1981.

[12] C. Liang, D. Zhang, Y. Zhou, X. Shu, S. Che, and C. Liu, "Coupling effect of a single-mode fiber coil under time-varying temperature and magnetic field," *J. Lightw. Technol.*, vol. 37, no. 13, pp. 3208-3212, Jul. 2019.

[13] J-I Sakai and T. Kimura, "Polarization behavior in multiply perturbed single-mode fibers," *IEEE J. Quantum Electron.*, vol. 18, no. 1, pp. 59-64, Jan. 1982.

[14] S. C. Rashleigh, "Origins and controls of polarization effects in single-mode fibers," *J. Lightw. Technol.*, vol. 1, no. 2, pp. 312-331, Jun. 1983.

[15] J. Noda, K. Okamoto, and Y. Sasaki, “Polarization-maintaining fibers and their applications”, *J. Lightw. Technol*., vol. 4, no. 8, pp. 1071-1085, Aug. 1986.
[16] J. Liu and T. Xu, “Revisiting the stress-induced birefringence in polarization-maintaining fibers,” *J. Lightw. Technol.*, vol. 41, no. 15, pp. 5097-5106, Aug. 2023.
[17] J. Liu Y. Liu, and T. Xu, “Analytical estimation of stress-induced birefringence in Panda-type polarization-maintaining fibers,” *IEEE Photon. Technol. Lett*., vol. 32, no. 24, pp. 1507-1510, Dec. 2020.
[18] W. K. Burns, R. P. Moeller, C. A. Villarruel, and M. Abebe, “Fiber-optic gyroscope with Polarization-holding fiber,” *Opt. Lett*., vol. 8, no. 10, pp. 540-542, Oct. 1983.
[19] W. Burns, “Phase error bounds of fiber gyro with polarization-holding fiber,” *J. Lightw. Technol*. vol. 4, no. 1, pp. 8-14, Jan. 1986.
[20] J. Liu and T. Xu, “Theoretical analysis of the non-reciprocal phase shift due to birefringence and topology in fiber ring interferometers,” *Opt. Laser Technol*., vol. 142, May 2021, Art. no. 107249.
[21] J. Liu, Y. Liu, and T. Xu, “Bias error and its thermal drift due to fiber birefringence in interferometric fiber-optic gyroscopes,” *Opt. Fib. Technol.*, vol. 55, Feb. 2020, Art. no. 102138.
[22] K. Tadaka, K. Okamoto, Y. Sasaki, and J. Noda, “Ultimate limit of polarization cross talk in birefringent polarization-maintaining fibers,” *J. Opt. Soc. Am. A*, vol. 3, no. 10, pp. 1594-1603, Oct. 1986.
[23] M. Tsubokawa, T. Higashi, and Y. Sasaki, “Measurement of mode couplings and extinction ratio in polarization-maintaining fibers,” *J. Lightw. Technol.*, vol. 7, no. 1, pp. 45-50, Jan. 1989.
[24] R. Liao, M. Tang, S. Fu, and D. Liu, “Distributed measurement of polarization mode coupling in polarization maintaining fiber using microwave photonic filter technique,” *J. Lightw. Technol*., vol. 36, no. 19, pp. 4543-4548, Oct. 2019.
[25] Z. Li, X. S. Yao, X. Chen, X. Chen, Z. Meng, and T. Liu, “Complete characterization of polarization-maintaining fibers using distributed polarization analysis,” *J. Lightw. Technol.*, vol. 33, no. 2, pp. 372-380, Jan. 2015.
[26] F. P. Kapron, N. F. Borrelli, and D. B. Keck, “Birefringence in dielectric optical waveguides,” *IEEE J. Quantum Electron*., vol. 8, no.2, pp. 222-225, Feb. 1972.
[27] K. Hotate and K. Tabe, “Drift of and optical fiber gyroscope caused by the Farady effect: influence of the earth’s magnetic field,” *Appl. Opt.*, vol. 25, vol. 7, pp. 1086-1092, Jul. 1986.
[28] R. C. Jones, “A new calculus for the treatment of optical systems I. Description and discussion of the calculus,” *J. Opt. Soc. Am.*, vol. 31, pp. 488-493, Jul. 1941.
[29] R. A. Campos and B. E. A. Saleh, “Quantum-mechanical lossless beam splitter: SU(2) symmetry and photon statistics,” *Phys. Rev. A*, vol. 40, no. 3, pp. 1371-1384, Aug. 1989.